Color filter array design using random patterns with blue noise chromatic spectra

Laurent Condat *

GREYC, 6 Bd. Maréchal Juin, 14050 Caen cedex, France

ARTICLE INFO

ABSTRACT

We propose two new types of random patterns with R, G, B colors, which allow to design color filter arrays (CFAs) with good spectral properties. Indeed, the chrominance channels have blue noise characteristics, a property which maximizes the robustness of the acquisition system to aliasing. With these new CFAs, the demosaicking artifacts appear as incoherent noise, which is less visually disturbing than the moiré structures characteristic of CFAs with periodic patterns.

© 2009 Elsevier B.V. All rights reserved.

1. Introduction

At the heart of color imaging systems like digital cameras is a sensor on which a *color filter array* (CFA) is overlaid [1]. The most popular is the Bayer CFA [2], which consists in red (R), green (G), and blue (B) filters arranged periodically. Given the mosaicked image acquired by the sensor, some processing is required to reconstruct a full color image with complete R, G, B components. This operation, called *demosaicking*, is generally achieved through interpolation techniques, see e.g. [1,3–7] and references therein. While the optimization of the demosaicking process has been studied extensively, the design of new CFAs with improved performances over the Bayer CFA has been ignored in the literature until recently. Indeed, this CFA is known to yield moiré artifacts in regions of the image with horizontally or vertically aligned structures [3]. Using other periodic CFAs with R, G, B filters may eliminate the presence of artifacts in some parts of the demosaicked image, while degrading the quality in other parts [8]. Recent advances have shown that using colors other than R, G, B, CFAs with much better robustness to aliasing can be designed [9,10]. However, the physical realizability of such CFAs may be problematic.

In this work, we explore another strategy, which mimics the human visual system: we consider CFAs with R, G, B filters, but with random arrangements. Since the acquisition of a color image through a CFA necessarily implies some lossy undersampling operation, aliasing issues are unavoidable. However, it is known, especially for printing [11] and computer graphics applications [12],

that random sampling yields images where aliasing artifacts appear as incoherent noise, which is more pleasing and less visible than coherent moiré structures [13,14]. The necessary condition for aliasing to appear as noise is to avoid low frequencies in the sampling patterns associated to each of the R, G, B components of the CFA. Based on the spectral characterization of the mosaicking process [3,9], we justify in Section 2 the choice of CFAs whose color channels have such blue noise characteristics—A 2-D blue noise spectrum is characterized by a concentration of energy beyond some radius from the origin in the frequency domain. R, G, B sampling with a random blue noise pattern is a good model of how the information is captured by the human visual system [15]. We propose in Section 3 two different approaches for the difficult problem of generating three mutually exclusive R, G, B random patterns having the same desired spectral characteristics. We evaluate their performances in Section 4 using three generic demosaicking algorithms.

2. Spectral properties of CFAs

2.1. Mathematical preliminaries

In this article, boldface letters denote vectors, e.g. $\mathbf{k} = [k_1, k_2]^T \in \mathbb{Z}^2$, $\mathbf{0} = [0, 0]^T$, $\boldsymbol{\pi} = [\pi, \pi]^T$. A CFA with R, G, B filters is a color image $\mathbf{cfa} = (\mathbf{cfa}[\mathbf{k}])_{\mathbf{k} \in \mathbb{Z}^2}$, where $\mathbf{cfa}[\mathbf{k}] \in \{\mathbf{R}, \mathbf{G}, \mathbf{B}\}$ is the color of the filter at location $\mathbf{k} \in \mathbb{Z}^2$ and $\mathbf{R} = [1, 0, 0]^T$, $\mathbf{G} = [0, 1, 0]^T$, $\mathbf{B} = [0, 0, 1]^T$. The *mosaicked* image $v = (v[\mathbf{k}])_{\mathbf{k} \in \mathbb{Z}^2}$ acquired by the sensor is such that $v[\mathbf{k}] = \mathbf{im}[\mathbf{k}]^T \mathbf{cfa}[\mathbf{k}]$ for every $\mathbf{k} \in \mathbb{Z}^2$, where the color image $\mathbf{im} = (\mathbf{im}[\mathbf{k}])_{\mathbf{k} \in \mathbb{Z}^2}$ is the ground truth to be estimated by demosaicking. That is, $\mathbf{im}[\mathbf{k}]$ is the vector of the three R, G, B values that would have been obtained if three measurements had been performed

* Tel.: +33 231452922.
  E-mail address: laurent.condat@greyc.ensicaen.fr

using R, G, B filters in front of the sensor at location $\mathbf{k}$, We define the Fourier transform of a signal $g = (g[\mathbf{k}])_{\mathbf{k} \in \mathbb{Z}^2}$ as $\hat{g}(\omega) = \sum_{\mathbf{k} \in \mathbb{Z}^2} g[\mathbf{k}] e^{-j\omega^T \mathbf{k}}$. $*$ denotes the convolution.

It is well known that in natural images, the R, G, B components are not independent [16,4,6,1,17]. Thus, we consider instead the orthonormal basis corresponding to luminance, red–green (R–G) and blue–yellow (B–Y) chrominance, defined as

$$L = \frac{1}{\sqrt{3}}[1, 1, 1]^T, \; C_1 = \frac{1}{\sqrt{2}}[-1, 1, 0]^T, \; C_2 = \frac{1}{\sqrt{6}}[-1, -1, 2]. \tag{1}$$

We denote g^L, g^{C_1}, and g^{C_2} the components of a color signal $\mathbf{g}$ in this basis. These components can be considered statistically independent for natural images [16].

In order to analyse the properties of the Bayer CFA, Alleysson et al. showed that the mosaicked image v can be interpreted, in the Fourier domain, as the sum of the luminance and chrominance components of the color reference image $\mathbf{im}$, moved at different locations of the frequency plane [3]. This characterization can be extended to every CFA. In our notations, from $v[\mathbf{k}] = \mathrm{im}^L[\mathbf{k}] \, \mathrm{cfa}^L[\mathbf{k}] + \mathrm{im}^{C_1}[\mathbf{k}] \, \mathrm{cfa}^{C_1}[\mathbf{k}] + \mathrm{im}^{C_2}[\mathbf{k}]\mathrm{cfa}^{C_2}[\mathbf{k}]$ and $\mathrm{cfa}^L[\mathbf{k}] = 1/\sqrt{3}$ for every $\mathbf{k}$, we get:

$$\hat{v}(\omega) = \frac{1}{\sqrt{3}} \widehat{\mathrm{im}^L}(\omega) + \sum_{C \in \{C_1, C_2\}} \widehat{\mathrm{im}^C}(\omega) \; * \; \widehat{\mathrm{cfa}^C}(\omega), \quad \omega \in \mathbb{R}^2. \tag{2}$$

2.2. The goal of CFA design

Since the signals im^L, im^{C_1} and im^{C_2} are lowpass, the best way for reducing the overlap between the chrominance and luminance signals, which is the cause of most of the artifacts in the demosaicked image [3], is to reject the chrominance in the corners of the Nyquist band, around the frequency π. But $\widehat{\mathrm{cfa}^{C_1}}$ and $\widehat{\mathrm{cfa}^{C_2}}$ can not both be Dirac distributions at π: this configuration would correspond spatially to a bi-colored checkerboard, with one of the two chrominance information completely lost. For a periodic CFA, $\widehat{\mathrm{cfa}^{C_1}}$ and $\widehat{\mathrm{cfa}^{C_2}}$ are sums of Dirac distributions, located on the dual lattice of the spatial lattice underlying the periodicity of the CFA [9]. This limitation does not hold for aperiodic patterns. This observation formed the basis of our motivation for seeking a CFA with a random pattern and chrominance having blue noise characteristics; that is, minimal energy in the baseband and all its energy concentrated around π. Thus, cfa^{C_1} and cfa^{C_2} should have similar (but orthogonal) spectra, close but not equal to Dirac distributions at π, so that the chrominance information is fairly encoded in the mosaicked image without preferential color axis.

In the case of the Bayer CFA, the chrominance is located in the frequency plane at the frequencies π, $[0, \pi]^T$, $[\pi, 0]^T$, and $\mathbf{0}$ [3], as illustrated in Fig. 1a. The presence of chrominance energy at $[0, \pi]^T$ and $[\pi, 0]^T$ is responsible for the moiré artifacts that appear in areas of the image with horizontal or vertical high-frequency content [3,9]. Aliasing between the high-frequency content of the luminance and the chrominance around these two frequencies is visible in the example of Fig. 1b. Moreover, a CFA without preferred color axis (that is, with one third of R, of G, and of B filters) is better, since the luminance im^L is not corrupted by chrominance in the baseband of v and can be optimally recovered during demosaicking.

2.3. Blue noise patterns

A 2-D blue noise spectrum is characterized by a concentration of energy beyond some radius from the origin in the frequency domain [11]. For example, a Poisson disk distribution is a blue noise pattern that can be defined as the limit of a uniform sampling process with a minimum-distance rejection criterion that cancels the low-frequency content of the pattern [19,14]. In our context, we look for patterns which are sub-domains of the regular square lattice. So, to mimic the behavior of Poisson disk distributions, we define the minimum-distance criterion as the property that two adjacent CFA filters have different colors. This ensures that the low-frequency content in the chrominance is canceled out. A straightforward implementation that yields a Poisson disk distribution, known as *dart throwing* [14,19], consists in adding pixels one by one to the distribution; the location of a new pixel is chosen randomly with a uniform distribution and the pixel is added if it is not closer than the desired distance from all pixels already in the set. However, as more and more pixels are added, the open area where samples can be added becomes arbitrarily small and an increasing large number of candidates are rejected before a new pixel is added to the set. This makes dart throwing really inefficient. More problematic is the fact than in our context, where every pixel of the pattern has to be affected a color, there are, after dart throwing, free locations where no color could be affected, because they already have neighbors with the three colors. Thus, dart throwing fails to generate a tri-colored mosaic where any two adjacent pixels have different colors.

To our knowledge, only the work of Zhu and Parker has addressed the problem of designing random R, G, B patterns with blue noise characteristics, using blue noise masks thresholded at different levels [20]. A blue noise mask is a greyscale pattern which, when thresholded at any value T, provides a binary pattern with mean value T and approximate blue noise spectrum [21].

    (a)   (b)
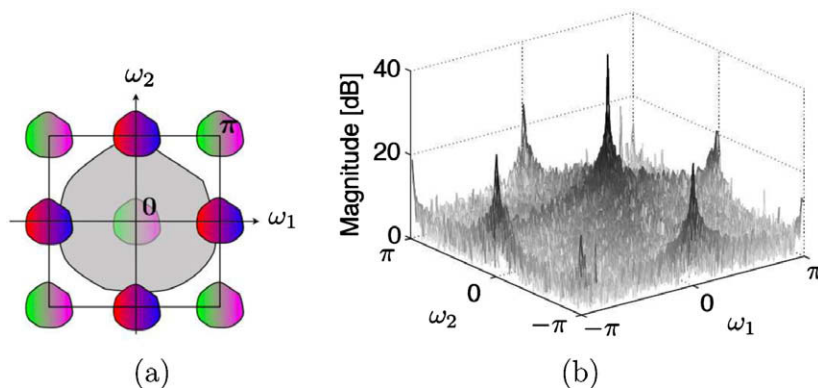
Fig. 1. Schematic representation of the spectrum of a mosaicked image sampled using the Bayer CFA (a), showing that the luminance (in gray) occupies the baseband while the chrominance (in color) is modulated at the frequencies π, $[0, \pi]^T$, $[\pi, 0]^T$, and $\mathbf{0}$. In (b), spectrum of the mosaicked *Lighthouse* image (figure borrowed from [18]).

However, these strong requirement prevents each given pattern, at fixed T, to have optimal spectral characteristics. The small example given in [20, Fig. 18b] clearly shows clusters of adjacent pixels with the same color. Moreover, if the red and blue pattern have blue noise characteristics, this is not clear that this also holds for the green channel with their approach.

3. Two new methods generating random patterns with blue noise characteristics

3.1. Method 1 – Improved tri-color dart throwing

The first method we propose is a modified dart throwing strategy adapted to our context. It consists in three steps:

1. We first generate a random permutation over the set of all possible pixel locations. We run through the obtained sequence of locations and add the pixels one by one. For each pixel, the color is chosen randomly, under the constraint that it is different from the colors of the already placed neighbors, whenever possible.
2. After step 1, about one in every four pixels has a neighbor with the same color. The second step, which is iterative, aims at correcting these "bad" pixels. At each iteration, we run through a random permutation over the set of all pixel locations. For each considered pixel, if one or more of its neighbors has the same color, we change its color. We do not have any guarantee that this process converges, but we found out that the number of bad pixels seems to decay logarithmically with the number of iterations. Experimentally, we used 1000 iterations to generate our mosaics, with still about 0.1% of remaining bad pixels.
3. The third step consists in changing some pixel values so that local bi-colored checkerboards become tri-colored Bayer-like patterns. We process the pixels in scanline order and change the value of a pixel if its four neighbors have the same color and three or more of its diagonal pixels have the same color. The third color, different from the one of all these neighbors, is assigned to the pixel.

This final step slightly improves the spectral characteristics of the mosaic. Additionally, it ensures that in every 3×3 bloc of the mosaic, there are at least one and at most four pixels for each color. This may simplify the demosaicking process, since there is no large area without information in one color band.

3.2. Method 2 – Fast random tiling

Since the previous method is quite slow—although this is not really an issue since the pattern has to be created once and for all—we investigated another strategy for quickly generating mosaics without any two adjacent pixels having the same color. This second approach, described in [22], is very fast. It consists in filling in the mosaic in scanline order, in two steps:

1. The first row of the mosaic is generated in scanline order, by adding successively tiles of three pixels chosen among the following six tiles:

$$1: [R, G, B] \quad 2: [R, B, G] \quad 3: [G, B, R] \tag{3}$$
$$4: [G, R, B] \quad 5: [B, R, G] \quad 6: [B, G, R] \tag{4}$$

Each new tile is chosen randomly among two possible tiles, depending on the tile at its left. The admissible adjacent combinations are:

$$1 \rightarrow \{2, 4\}, \quad 2 \rightarrow \{1, 5\}, \quad 3 \rightarrow \{4, 6\}, \tag{5}$$
$$4 \rightarrow \{1, 3\}, \quad 5 \rightarrow \{2, 6\}, \quad 6 \rightarrow \{3, 5\}. \tag{6}$$

For example, at the right of a tile 1, we have the choice between the tiles 2 and 4. The first column of the mosaic is generated the same way, using vertical 3-tiles.
2. The mosaic is then filled in, in scanline order. Each pixel receives a color different from the ones of its left and top neighbors. If two colors are possible, we assign the color different from the one of the top-left diagonal neighbor. So, this second step is deterministic.

Using this method, we obtain an aperiodic tiling of the whole image with tri-colored diamonds, as illustrated in Fig. 3a. The choice of using 3-tiles is empirical, but has been found to yield the best results among numerous other methods tried.

4. Performance analysis

4.1. Spectral analysis

Examples of the random mosaics obtained using the two algorithms are depicted in Figs. 2 and 3, as well as the amplitude spectra of their B–Y chrominance components. The spectra were obtained by smoothing the amplitude of the FFT with a 5×5 box

(a)   (b)   (c)
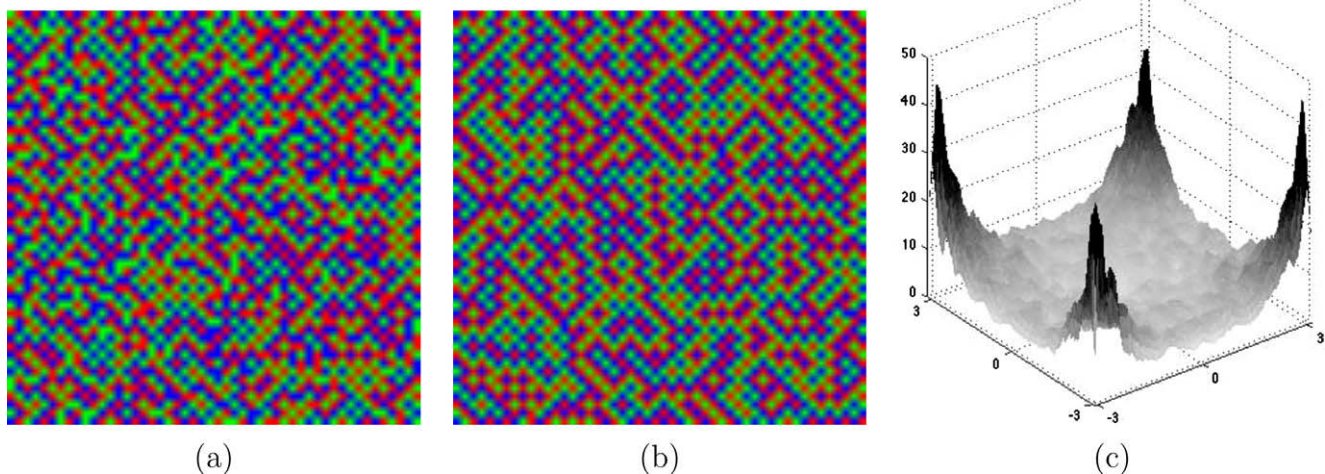
Fig. 2. Parts of the mosaic of size 100×100 generated by the algorithm described in Section 3.1, after step 1 (a) and step 3 (b). The (smoothed) magnitude of the FFT for the B–Y chrominance of the mosaic after step 3 is depicted in (c).
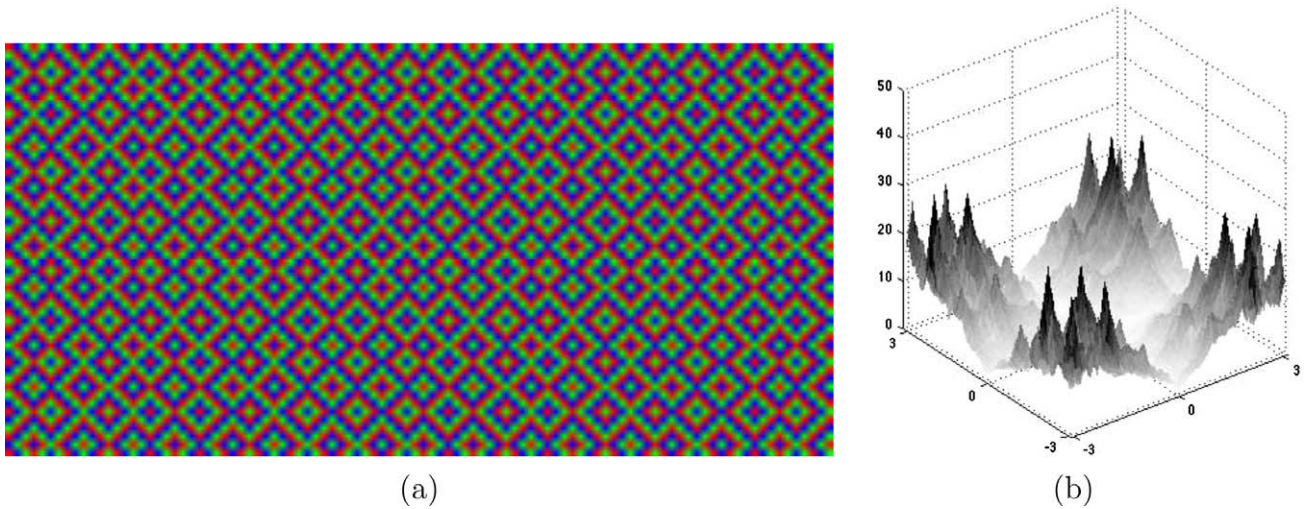
Fig. 3. Part of the mosaic of size 100 × 100 generated by the algorithm described in Section 3.2 (a) and the (smoothed) magnitude of the FFT for the B–Y chrominance of the mosaic (b).

Table 1
Mean square error for the demosaicking experiments using the different combinations of CFAs (Bayer, two proposed designs) and demosaicking methods (3 × 3 normalized convolution denoted "bilinear", methods of [5,23]). Image numbers are the same as in [7].

| Image | Bayer | | | | | Proposed CFAs | | | | | |
| | Bilinear | [5] | [23] | [24] | [25] | Type I | | | Type II | | |
						Bilinear	[5]	[23]	Bilinear	[5]	[23]
1	151.66	15.77	13.74	11.45	10.12	158.04	28.49	13.89	141.04	22.62	11.37
2	29.87	6.56	13.74	5.75	6.80	33.19	9.83	11.24	30.08	8.60	10.14
3	137.23	15.32	18.43	10.14	10.56	164.40	35.38	24.36	145.97	32.24	22.32
4	105.15	12.45	10.89	10.15	6.47	111.21	20.08	10.83	101.11	17.15	9.23
5	28.79	5.02	7.95	3.34	4.00	35.36	9.63	8.23	30.28	8.06	7.58
6	277.64	31.72	30.59	19.26	19.31	285.55	51.53	25.20	251.79	37.91	19.22
7	36.33	5.37	6.66	3.38	3.96	40.73	9.61	6.90	35.19	7.69	6.15
8	36.34	4.81	5.49	3.56	3.91	41.75	9.61	6.61	36.78	8.31	5.99
9	76.71	9.17	10.39	7.49	6.80	83.32	16.48	10.89	75.28	14.43	9.86
10	28.98	4.53	5.39	3.39	3.20	30.79	7.03	5.15	27.29	5.72	4.46
11	262.85	27.75	20.64	27.03	19.98	285.79	51.52	27.90	266.80	49.98	26.75
12	32.01	7.80	11.01	7.06	7.35	37.35	12.25	11.09	33.29	10.85	10.24
13	47.17	6.03	5.42	4.92	2.77	48.63	8.64	4.72	44.12	7.26	3.98
14	39.07	5.41	5.81	4.66	4.42	45.42	10.12	6.75	40.72	9.44	6.25
15	101.74	14.96	15.77	13.01	12.05	114.24	26.23	18.43	103.07	24.27	17.21
16	100.30	11.12	11.09	6.30	5.92	103.15	18.87	9.83	90.92	14.35	7.75
17	43.88	6.47	8.95	5.04	5.92	50.29	11.39	8.89	44.98	10.26	8.07
18	89.82	10.66	10.32	8.72	8.51	98.42	18.46	11.11	88.56	16.35	9.87
19	57.14	12.02	14.40	9.00	9.86	62.89	17.56	14.57	56.66	15.75	13.60
20	136.93	24.37	23.37	21.42	18.94	151.50	36.99	27.37	139.03	35.53	26.19
Average	90.98	11.87	12.50	9.25	8.54	94.60	20.49	13.20	89.15	17.84	11.81

filter. The R–G chrominance channel has the same spectrum as the B–Y one, up to random fluctuations. As expected, the first algorithm provides spectra with blue noise characteristics. The energy is well concentrated around π. The amount of energy in the low-frequency part is not negligible, however.

The second algorithm yields mosaics with less chrominance energy around the origin and a high-frequency content spread in the area $[-\pi, \pi]^2 \setminus [-2\pi/3, 2\pi/3]^2$. The mosaic is also more structured and anisotropic than with the first approach.

We note that whatever the strategy used for generating a random pattern, there seems to exist some balance between how well the chrominance energy is concentrated around π and the amount of chrominance energy around the zero frequency. This may be explained by the fact that energy at π correspond to local bi-colored checkerboard patterns in the mosaic, which also have low-frequency chrominance content. The effect of the step 3 of the first

algorithm is to decrease the energy of the chrominance around **0** and π and to increase the energy around $[0, \pi]^T$ and $[\pi, 0]^T$.

4.2. Practical demosaicking experiments

In order to validate our designs experimentally, we considered the data set of 20 color images of size 768 × 512 used by many authors to test their methods (e.g. [7,9]). These images were mosaicked using the proposed CFAs and the Bayer CFA, and demosaicked using three different methods:

1. We propose a simple linear scheme that consists in computing a missing value for the color $\mathbf{C} \in \{\mathbf{R}, \mathbf{G}, \mathbf{B}\}$ at location $\mathbf{k}$, by averaging the pixel values $v[\mathbf{l}]$ for $\mathbf{l}$ in a 3 × 3 neighborhood surrounding $\mathbf{k}$ and for which $h[\mathbf{l}] = \mathbf{C}$. This simple scheme reverts to bilinear interpolation for the Bayer pattern.

Fig. 4. Part of the demosaicked image *lighthouse* (image 16 in Table 1), for different combinations of CFA (each column) and demosaicking method (each row).

2. We implemented the non-linear demosaicking algorithm of Lukac and Plataniotis [5] which is, to our knowledge, the only advanced demosaicking algorithm proposed in the literature, that can be used for every R, G, B CFA. The G plane is first interpolated incrementally using an edge-sensitive process. The B and R planes are then reconstructed using the G plane, based

on a model that takes into account the spectral correlations between the R, G, B components. Finally, a post-processing step updates the G plane from the computed B and R planes.

3. We developed a new linear demosaicking algorithm, that can be applied to every CFA [23]. It is based on a variational framework: the image with maximal smoothess interpolating the data is computed. More precisely, the iterative process converges to the image **u** which is consistent with the measurements $v[\mathbf{k}]$ while minimizing the quadratic criterion $\mu\|\nabla u^L\|^2 + \|\nabla u^{C_1}\|^2 + \|\nabla u^{C_2}\|^2$. The parameter μ plays a key role; it enforces the chrominance to be smoother than the luminance, a known property of natural images. $\mu = 0.04$ turns out to give the best results experimentally, for the proposed CFAs and the Bayer CFA as well.

The numerical results for every combination of CFAs and demosaicking methods are summarized in Table 1.[1] We first observe that the simple linear demosaicking method, which does not exploit the cross-correlations between the color bands in natural images, provides relatively poor results. Our random CFA outperforms the Bayer CFA by a small margin. The demosaicking method of Lukac yields a much better quality. The best performances are obtained with the Bayer CFA, but there might be a bias if this method has precisely been tuned to perform well with this CFA in particular. The new demosaicking method developed in [23] performs globally best, although the one of Lukac remains better for the Bayer CFA only. Note that the first and third demosaicking methods are linear; hence, their results are more reliable indications of the intrinsic quality of the CFAs under test. As a result, the proposed CFA of type 2 slightly outperforms the Bayer CFA, while the proposed CFA of type 1 is slightly behind them.

We also included in Table 1 the results of the two methods presented in [24,25], which represent the state of the art of demosaicking for the Bayer CFA. These results show the improvements achievable by methods sophisticated but specifically tuned for the Bayer CFA over the three basic but generic methods described above. It is probable that similar improvements could be obtained for demosaicking with the new random CFAs, if efforts were deployed to adapt the mechanisms of the best methods to them.

A visual inspection of the demosaicked images allows to balance the numerical results with the real disturbance of the aliasing artifacts characteristic to each CFA. In Fig. 4, we show the fence in the *lighthouse* image, often used as benchmark for comparing demosaicking results. Due to the superposition of the chrominance and luminance in the mosaicked image according to Eq. (2), most of the visible artifacts come from an incorrect assignment of information corresponding to high-frequency content of luminance to the chrominance during demosaicking. In this respect, the artifacts present with the random CFA take the form of chrominance noise, which is more visually pleasant than the structured low-frequency color fringes characteristic to the Bayer CFA. Even with the demosaicking method of [5], which provides a lower MSE for the Bayer pattern, the artifacts are less visible with the random CFAs.

We note that the type 2 random CFA is superior to the type 1, both numerically and visually. This suggests that, in first place, the energy of the CFA in the chrominance channels has to be minimal in the baseband, where the luminance information is located in the frequency plane. This property seems to be more important that a good concentration of the energy around π.

5. Conclusion

We proposed two methods for generating R, G, B CFAs with random patterns, such that two adjacent pixels have different colors. This property ensures that the chrominance channels have reduced energy in the low frequency area, a necessary property to minimize aliasing. In comparison with the Bayer CFA, or every other periodic R, G, B CFA, the new random CFAs yield less disturbing demosaicking artifacts, which appear as incoherent chromatic noise. In practice, a small random pattern (e.g. of size 16×16) can be designed with one of our two methods and periodically replicated to form the pattern of a pseudo-random CFA. The physical realizability would be made easier and the performances would be almost unchanged. For reproducibility purpose, Matlab code generating the proposed random patterns has been made available online.[2]

As future work, the development of random patterns with even better spectral properties should be investigated. Indeed, we believe that there exists some margin of improvement over the two designs presented in this paper, toward a random pattern with an isotropic growth of the chrominance energy away from **0** and a peak of energy around π. The design of demosaicking methods able to exploit these patterns at best should be studied as well.

The proposed framework can be extended to multispectral imaging, in which more than three bands are acquired, e.g., visible and infrared bands in remote sensing systems. Also, there may be other applications for random color patterns, like multitone dithering in printing [26] and texture generation in computer graphics [27]. Thus, we wish the present work to foster a renewed interest for random color sampling.

Acknowledgments

References

[1] B.K. Gunturk, J. Glotzbach, Y. Altunbasak, R.W. Schaffer, R.M. Mersereau, Demosaicking: color filter array interpolation, IEEE Signal Process. Mag. 22 (1) (2005) 44–54.
[2] B.E. Bayer, Color imaging array, US patent no. 3971065, July 1976.
[3] D. Alleysson, S. Süsstrunk, J. Hérault, Linear demosaicing inspired by the human visual system, IEEE Trans. Image Process. 14 (4) (2005) 439–449.
[4] J. Portilla, D. Otaduy, C. Dorronsoro, Low-complexity linear demosaicing using joint spatial–chromatic image statistics, in: Proceedings of IEEE ICIP, 2005.
[5] R. Lukac, K.N. Plataniotis, Universal demosaicking for imaging pipelines with a RGB color filter array, Pattern Recogn. 38 (2005) 2208–2212.
[6] S.C. Pei, I.K. Tam, Effective color interpolation in CCD color filter arrays using signal correlation, IEEE Trans. Circuits Syst. Video Technol. 13 (2003) 503–513.
[7] B.K. Gunturk, Y. Altunbasak, R.M. Mersereau, Color plane interpolation using alternating projections, Proc. IEEE 11 (9) (2002) 997–1013.
[8] R. Lukac, K.N. Plataniotis, Color filter arrays: design and performance analysis, IEEE Trans. Consum. Electron. 51 (4) (2005) 1260–1267.
[9] K. Hirakawa, P.J. Wolfe, Spatio-spectral color filter array design for optimal image recovery, IEEE Trans. Image Process. 17 (10) (2008) 1876–1890.
[10] L. Condat, A new color filter array with optimal sensing properties, in: Proceedings of IEEE ICIP, 2009.
[11] R.A. Ulichney, Dithering with blue noise, Proc. IEEE 76 (1) (1988) 56–79.
[12] A. Glassner, Principles of Digital Image Synthesis, Morgan Kaufman Publishers, 1995.
[13] M. Dippé, E. Wold, Antialiasing through stochastic sampling, in: Proceedings of SIGGRAPH, 1985, pp. 69–78.
[14] D. Mitchell, Generating antialiased images at low sampling densities, in: Proceedings of SIGGRAPH, 1987, pp. 65–72.
[15] J.I.J. Yellot, Spectral consequences of photoreceptor sampling in the rhesus retina, Science (1983) 382–385.
[16] Y. Hel-Or, The canonical correlations of color images and their use for

---

[1] We do not take into account the first and last five rows and columns of the demosaicked images for the computation of the MSE, since the initial images used for the tests have been badly acquired at the boundaries.

demosaicing, Tech. Rep. HPL-2003-164R1, HP Laboratories Israel, February 2004.

[17] B.A. Wandell, Foundations of Vision, Sinauer Associates, Inc., 1995.

[18] D. Menon, Color image reconstruction for digital cameras, Ph.D. thesis, University of Padova, Italy, 2009.

[19] M. McCool, E. Fiume, Hierarchical poisson disk sampling distributions, in: Proceedings of Graphics Interface, 1992, pp. 94–105.

[20] W. Zhu, K. Parker, M.A. Kriss, Color filter arrays based on mutually exclusive blue noise patterns, J. Vis. Commun. Image Represent. 10 (3) (1999) 245–267.

[21] T. Mitsa, K. Parker, Digital halftoning technique using a blue-noise mask, J. Opt. Soc. Am. 9 (11) (1992) 1920–1929.

[22] L. Condat, A new random color filter array with good spectral properties, in: Proceedings of IEEE ICIP, 2009.

[23] L. Condat, A generic variational approach for demosaicking from an arbitrary color filter array, in: Proceedings of IEEE ICIP, 2009.

[24] L. Nai-Xiang, C. Lanlan, T. Yap-Peng, V. Zagorodnov, Adaptive filtering for color filter array demosaicking, IEEE Trans. Image Process. 16 (10) (2007) 2515–2525.

[25] E. Dubois, Frequency-domain methods for demosaicking of Bayer-sampled color images, IEEE Signal Process. Lett. 12 (12) (2005) 847–850.

[26] J.B. Rodríguez, G.R. Arce, D.L. Lau, Blue-noise multitone dithering, IEEE Trans. Image Process. 17 (8) (2008) 245–267.

[27] M.F. Cohen, J. Shade, S. Hiller, O. Deussen, Wang tiles for image and texture generation, in: Proceedings of SIGGRAPH, 2003, pp. 287–294.